A PRELIMINARY STUDY ON SIMULATIONS OF A SINGLE JET FROM THE ECN "SPRAY G" TEST CASE

Mateus Dias Ribeiro ✉, mateusdias@feg.unesp.br
Alex Mendonça Bimbato, alexbimbato@feg.unesp.br
Maurício Araújo Zanardi, mzanardi@feg.unesp.br
José Antônio Perrella Balestieri, perrella@feg.unesp.br

FEG - UNESP, Av. Dr. Ariberto Pereira da Cunha, 333, Portal das Colinas, CEP 12.516-410, Guaratinguetá, São Paulo, Brazil

Abstract. *The direct injection spark ignition (DISI) engine has been often subject of research over the past few years due to its ability to reduce specific fuel consumption and achieve lower emissions. This has been mainly enabled by computational methods, that evolved rapidly over the years to allow detailed studies of the phenomena taking place in a gasoline direct injection engine, such as spray formation, heat transfer, evaporation and combustion. In this work, a Reynolds-Averaged Navier Stokes (RANS) methodology together with a Lagrangian Particle Tracking (LPT) approach were used to simulate one single jet of the "Spray G" multi-hole gasoline injection test case provided by the Engine Combustion Network (ECN). Each of the relevant physical phenomena were described in detail and included to the model. For the description of droplet breakup, the Reitz-Diwakar and the Reitz-KHRT models were employed and compared. The Ranz-Marshall model was used for the heat transfer between the liquid and gas phase and for the evaporation process flash-boiling is considered. Prelimary results are presented and discussed. The penetration length for both liquid and gas phase obtained by the RANS simulations were validated against experiments and good agreement was observed so far.*

Keywords: *Fuel-Spray, Internal Combustion Engine, RANS, Lagrangian, OpenFOAM*

1. INTRODUCTION

Worldwide legislations on greenhouse gases and pollutant emissions have become much more restrictive over the past years. Projections for the European CO_2 emissions target at a fleet average of 95 g/km for all new passenger cars by 2021. Whereas US standards set by EPA (United States Environmental Protection Agency) points out the value of 93 g/km by 2025. This information, as well information on projections for Mexico, Brazil, South Korea and other countries are well documented by The International Council on Clean Transportation (2014). Therefore, new technologies to improve efficiency and emissions of the new generation of passenger cars must be developed. Among these technologies are the direct injection spark ignition (DISI) engines.

The DISI engines aim to reduce the specific fuel consumption and achieve the strict emission standards in state of art internal combustion engines (Goryntsev et al. (2010); Peterson, Reuss, & Sick (2014)). The reduction of fuel consumption is achieved by directly injecting the fuel into the combustion chamber during the intake or compression stroke at very high injection pressures. When the fuel is injected within the compression stroke, the spray formed by the injector atomizer must change heat with the carrier phase, evaporate and mix with the gas inside the chamber in a very narrow period of time. This creates a region of high fuel concentration in the vicinity of the spark-plug and along the spray longitudinal axis. The fuel concentration decreases from rich until stoichiometric and lean conditions as long the distance from the spray core increases. This condition is known as stratified-charge combustion because it is expected that ignitable fuel concentrations exist only in a small region of the combustion chamber prior to ignition. Thus, under part load conditions, there is no need for a stoichiometric homogeneous fuel mixture over all the combustion chamber and the direct injection enables a large volume with very low or no fuel concentration at all, which potentially decreases the specific fuel consumption, eliminates load throttling and minimizes pumping losses (Baumgarten (2005)). Furthermore, fuel droplets evaporation cools down the charge in the chamber, allowing an increase of compression ratio in comparison to conventional spark ignition engines.

For higher loads, however, turbulence intensity increases considerably and stratified-combustion is no longer capable to deliver the necessary torque to the engine. The very high pressure and strong turbulence motions may cause the spray to collapse and a compact ignitable cloud next to the spark-plug will not be formed. In this case, stoichiometric or even fuel-rich mixture is needed and hence an early injection within the intake stroke will be necessary. In this way, it is possible to guarantee that the fuel will have enough time to mix adequately inside the chamber. Yang & Anderson (1998) considered the combined approach with late injection under part load and early injection under full load a good alternative to direct injection engines by combining the volumetric efficiency of the early one with the suppression of knock tendency of the latter. Zheng, Tian, & Zhang (2015) reported that a 25%-75% proportion for late and early injections, respectively, could be a reasonable configuration for low speed (1200 rpm) operation, due to the formation of a local, ignitable and rich mixture around the spark-plug leading to higher thermal efficiency and low soot emissions.

A key issue for developing DISI engines is the understanding of the physics of fuel-sprays and all the related phe-

nomena for their implementation in engines, such as injection, atomization, droplet breakup, collision, coalescence, heat transfer, mass transfer, momentum transfer, evaporation and so on. As experimental techniques (Peterson, Reuss, & Sick (2014)) still have limitations to capture and measure spray properties in optical engines and other experimental test-benches, computational methods on fuel-spray research have evolved rapidly over the last years, largely driven by growing computer power. A nice overview of recent developments in combustion modeling has been presented by Westbrook et al. (2005), pointing out how progress in the modeling of fluid dynamics, chemical kinetics, sprays and turbulence have helped to reduce the emission of harmful substances. A big variety of works have been published over the years using different techniques and computer codes to simulate evaporative/non-evaporative sprays and spray combustion (Vuorinen et al. (2011)); Lucchini, D'Errico, & Ettorre (2011); Jangi et al. (2015)). These works employ the Lagrangian Particle Tracking (LPT) approach to describe the fuel-spray droplets together with either a Reynolds Averaged Navier-Stokes (RANS) or Large-eddy Simulations (LES) model for the turbulence of the carrier phase. A good review on the progress of the LPT approach can be found in Subramaniam (2013) and Pope (2011).

In this work, we aim to make further contributions to the field of stratified-charge combustion in internal combustion engines by means of preliminary simulations of the "Spray G" condition, which corresponds to a non-reacting early injection case for spray-guided gasoline injection. Details about this condition and the means to validate the present code are discussed in section 3. In the next section, the modeling of the different phenomena related to fuel spray injection are described: modeling of the carrier phase, droplet formation and breakup, exchange of momentum with the carrier phase, heat/mass transfer and droplet vaporization.

2. SPRAY MODELING

The present work uses a Lagrangian-Eulerian methodology to model injection, breakup, heat-transfer, vaporization and mixture process with the carrier-phase of a gasoline spray. The environment (pressure and temperature) is set to be similar to an internal combustion engine combustion chamber at the end of the admission stroke. Therefore, the gas phase is assumed to be continuous and an Eulerian approach is used for its representation. The liquid phase, however, is composed of many discrete tiny droplets or particles, which are represented by means of a Lagrangian methodology.

2.1 Modeling of the gas phase

A Reynolds-Averaged Navier Stokes (RANS) approach was used to model the gas phase turbulence. Thus, the instantaneous quantities of the flow are decomposed into their time-averaged and fluctuating parts and the whole set of governing equations of the flow (continuity, momentum and energy) are averaged and solved. Only the mean quantities of the flow are resolved since the average of each fluctuating property is equal to zero and hence neglected. However, the Reynolds stress term does not vanish and must be modeled. For dealing with compressible flows, a change of variable is often applied for every quantity of interest φ, in which φ is density-weighted by the operation $\overline{\rho}\tilde{\varphi} = \overline{\rho\varphi}$. This is known as Favre-filtering and results in the Favre-filtered variable $\tilde{\varphi}$. In case of RANS, $\tilde{\varphi}$ represents a Favre-filtered of the averaged part of a quantity (like the velocity u). The whole set of the RANS equations for mass (1), momentum (2), energy (3) and species (4) conservation in the Favre-filtered form reads:

$$\frac{\partial \bar{\rho}}{\partial t} + \frac{\partial(\bar{\rho}\tilde{u_i})}{\partial x_i} = S_\rho \tag{1}$$

$$\begin{aligned}&\frac{\partial(\bar{\rho}\tilde{u_i})}{\partial t} + \frac{\partial(\bar{\rho}\tilde{u_i}\tilde{u_j})}{\partial x_j} = \\ &\frac{\partial}{\partial x_j}\left[\bar{\rho}\bar{\nu}\left(\frac{\partial \tilde{u_j}}{\partial x_i} + \frac{\partial \tilde{u_i}}{\partial x_j}\right) - \frac{2}{3}\bar{\rho}\bar{\nu}\frac{\partial \tilde{u_k}}{\partial x_k}\delta_{ij} - \frac{\partial}{\partial x_j}(\overline{\rho u_i'' u_k''})\right] - \frac{\partial \bar{p}}{\partial x_i} + \bar{\rho} g_i + S_u\end{aligned} \tag{2}$$

$$\frac{\partial(\bar{\rho}\tilde{h})}{\partial t} + \frac{\partial(\bar{\rho}\tilde{h}\tilde{u_j})}{\partial x_j} + \frac{\partial(\bar{\rho}\tilde{K})}{\partial t} + \frac{\partial(\bar{\rho}\tilde{K}\tilde{u_j})}{\partial x_j} = \frac{\partial}{\partial x_j}\left(\alpha_{eff}\frac{\partial \tilde{h}}{\partial x_j}\right) + \frac{\partial \bar{p}}{\partial t} + S_h \tag{3}$$

$$\frac{\partial(\bar{\rho}\tilde{Y_i})}{\partial t} + \frac{\partial(\bar{\rho}\tilde{Y_i}\tilde{u_j})}{\partial x_j} = \frac{\partial}{\partial x_j}\left(\mu_{eff}\frac{\partial \tilde{Y}}{\partial x_j}\right) + S_{Y_i} \tag{4}$$

The Reynolds Stress Term term $\overline{-\rho u_i'' u_k''}$ is modeled with the well established k-ϵ model. In the previous equations, u stands for velocity (in three spacial coordinates i, j and k), ρ is the fluid density, ν is dynamic viscosity, μ_{eff} is effective viscosity, α_{eff} is effective thermal diffusivity, p is pressure, h is enthalpy, K is kinetic energy, Y_i is mixture fraction of species i and S_ρ, S_u, S_h and S_{Y_i} are source terms needed to couple gas phase with particle phase. Finally, u_i'' represents the fluctuating part of the velocity u_i and and the bar symbol over variables represents averaging.

2.2 Modeling of the particle phase

In this work the parcel approach is used to reduce the computational effort. A full-cone (Fig. 1) spray is composed of a large number of particles of different diameters and handling each one of them would be very computational demanding. In order to circumvent the problem of simulating each particle separately, one can define a parcel as a group of droplets with the same properties, thus only bins of particles need to be treated numerically. Another reasonable assumption is to consider that all particles are perfectly spherical, having a diameter d. The size distribution of the injected droplets is modeled by the cumulative probability density function (CDF) Rosin-Rammer as shown in Eq. (5):

$$F(x,n,d) = 1 - e^{-(x/d)^n} \tag{5}$$

In this work, it was assumed constant of uniformity n = 3 and maximum and minimum droplet diameters were defined as 175 μm (approximately the size of the nozzle hole diameter) and 1.5 μm, respectively. For completeness d is the characteristic particle size and x is a particular particle size within the distribution.

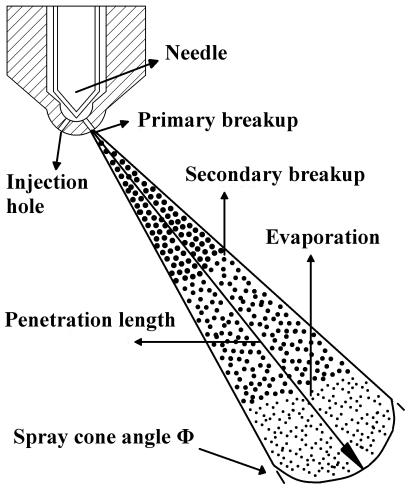

Figure 1: Schematic representation of a full-cone spray

The velocity magnitude of the injected parcels can be determined either by knowing the pressure drop between the injector nozzle and combustion chamber and applying the Bernoulli equation or by deriving it from the mass flow rate and injector geometry properties. Their direction can be correlated with expressions that distribute the parcels over a predefined range, in which small particles tend to be injected within an angle (not greater than a maximum predefined value) and the larger ones tend to go straight or within a small angle. When liquid fuel particles are injected at high velocities in a quiescent gas environment, they are decelerated by the gaseous environment. This exchange of momentum between liquid and gas phase takes place due to the relative velocity between them. Equation (6), as shown by Vuorinen et al. (2011), denotes the exchange of momentum by evaluating the resulting drag force over a liquid parcel moving with relative velocity $\mathrm{u_{res}}$ with respect to the gas phase.

$$\frac{1}{6}\rho_P \pi d^3 \frac{du_P}{dt} = \frac{1}{2}(u_g - u_P)|u_g - u_P|\rho_g C_D \frac{\pi d^2}{4} \tag{6}$$

The term on the left side in Eq. (6) represents the change of the acceleration of the liquid fuel particle, while the term on the right side denotes the drag force due to its relative motion to the gas phase. The subscript *g* refers to the gas phase and *P* to the liquid parcel of diameter d.

The drag coefficient $\mathrm{C_D}$ is calculated assuming spherical particles and is calculated using the Reynolds number of the gas phase $\mathrm{Re_g} = \mathrm{du_{rel}}\rho_\mathrm{g}/\mu_\mathrm{g}$. The correlation for evaluating $\mathrm{C_D}$ is presented in Eq. (7).

$$C_D = \begin{array}{l} \dfrac{24}{Re_g}\left(1 + \dfrac{1}{6}{Re_g}^{2/3}\right), Re \leq 1000 \\ 0.424, Re > 1000 \end{array} \tag{7}$$

Finally, the parcels can be tracked by updating their positions according to Eq. (8).

$$\frac{Dx_P}{Dt} = u_P \tag{8}$$

As soon as the liquid particles get into the domain, besides exchanging momentum, they also exchange heat with the gas phase. The liquid phase exchanges heat with the gas due to diffusive and convective transport and radiation. The heat exchange increases the temperature until the particle reaches the boiling temperature and evaporates. This is very important for the mixing process, combustion and formation of pollutants since the fuel starts to burn only when it is in the vapor phase.

In addition to the assumption of perfect spherical particles, one may also neglect the effect of radiation, since it is small compared to the convection. Furthermore, the evaporation modeling is based on the averaged flow field around the particles, because the flow among them is not feasible to be calculated.

Baumgarten (2005) obtains the following energy balance for a liquid particle, presented in Eq. (9):

$$m_P c_{p,l} \frac{dT_P}{dt} + \Delta h_{evap} \frac{dm_{evap}}{dt} = \lambda_g \pi d_P (T_\infty - T_P) \frac{\zeta}{e^\zeta - 1} Nu \tag{9}$$

The terms Nu and ζ are shown in Eq. (10) and Eq. (11), respectively.

$$Nu = \frac{\alpha d_P}{\lambda_g} \tag{10}$$

$$\zeta = \frac{\dot{m}_{evap} c_{p,vap}}{Nu \lambda_g \pi d_P} \tag{11}$$

Where T_∞ is the temperature of the gas phase and $\mathrm{T_P}$ is the temperature of the parcel, $\mathrm{d_P}$ is the parcel diameter, λ_g is the thermal diffusivity of the gas mixture, Nu is the Nusselt number and ζ is a dimensionless correction factor accounting of the reduced heat transfer due to the simultaneous mass transfer from the parcel to the gas phase. In Eq. (9), the first term represents the energy necessary to heat up the liquid fuel parcel until a given temperature in an interval dt, where $\mathrm{m_p}$ is the mass of the parcel, $\mathrm{T_P}$ its temperature and $\mathrm{c_{p,l}}$ the specific heat at constant pressure of the liquid fuel. The second term accounts for the energy necessary to evaporate the parcel mass $\mathrm{m_{evap}}$ during the interval dt. The term on the right hand side accounts for the heat transfer between the liquid and gas phase.

The appropriate Nusselt number, that accounts for the relative velocity between the particle and gas, is evaluated using the heat transfer correlation proposed by Marshall & Ranz (1952) and reads in Eq. (12):

$$Nu = 2.0 + 0.6 Re^{1/2} Pr^{1/3} \tag{12}$$

In this equation, the Reynolds number is denoted as Re and the Prantdl number as Pr, which are calculated with the properties of the gas phase.

Droplet vaporization is calculated by a model proposed by Zuo, Gomes, & Rutland (2000), which takes fuel droplet superheat vaporization into account. The model distinguishes between two kinds of vaporization. First, vaporization due to flash boiling and, second, vaporization due to normal heat transfer with the gaseous phase. For this, the Adachi's experimental (Adachi et al. (1997)) correlation is employed to calculate the drop flash vaporization rate.

2.2.1 Breakup modeling

The formation of droplets from a round continuous liquid jet can be distinguished among four different breakup regimes as shown in the work of Reitz & Bracco (1986): Rayleigh regime, first and second wind-induced regimes and atomization regime. The process of formation of these first droplets is known as primary breakup. Those droplets are then subject of secondary breakup, i.e., new particles are formed from the collapse of previous ones, due to high relative velocities between the gas/liquid interface. Baumgarten (2005) presents five different liquid drop breakup regimes: vibrational breakup (1), bag breakup (2), bag / streamer breakup (3), stripping breakup (4) and catastrophic breakup (5). Figure 2 illustrates the five breakup regimes according to Wierzba (1990).

The relative velocity between the liquid/gas interface induces aerodynamic forces that create oscillations in the droplet surface. The growing of the amplitude of these oscillations results on droplet breakup. The gas phase Weber number $\mathrm{We_g} = \mathrm{u^2_{rel} D \rho_g / \sigma}$ is the relevant parameter for the mechanism of liquid drop breakup. This number is a relation between the aerodynamic force, which tends to break up droplets into smaller particles and the surface tension force, which on the other hand tries to keep the parent droplets in their spherical shape. The $\mathrm{u^2_{rel}}$ is the relative velocity between particle and gas, D is the particle diameter, ρ_g is the gas density and σ is the droplet surface tension. As the droplets become smaller, the surface tension necessary to break it up becomes bigger and therefore the relative velocity must also be bigger to disintegrate the drop.

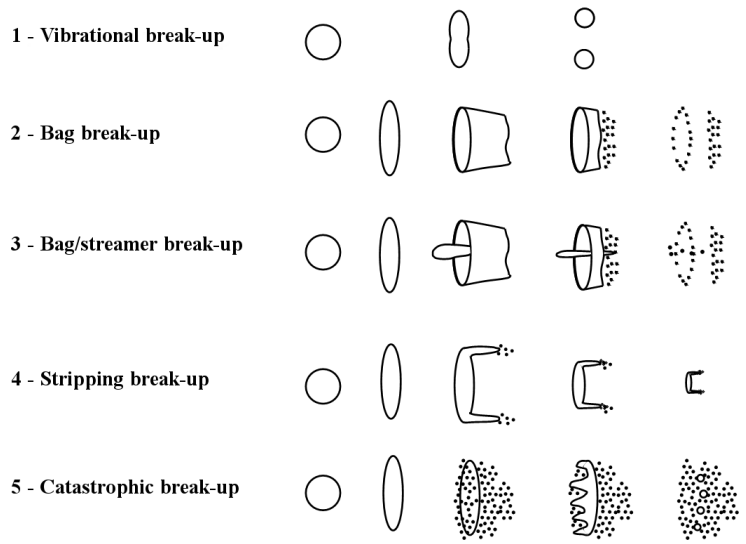

Figure 2: Droplet breakup according to Wierzba (1990)

Experimental investigations show that distinct breakup regimes can be divided according to a range of Weber numbers. Table 1 presents the transition Weber numbers for different breakup regimes. Regarding the numerical simulation of primary and secondary breakup processes, several models have been proposed in the literature. In the present work, two breakup models have been tested: The Reitz-Diwakar model (Reitz (1987)) and the Reitz-Kelvin-Helmholtz/Rayleigh-Taylor model (Beale & Reitz (1999)).

Table 1: Transition Weber numbers for different regimes as in Baumgarten (2005)

Wierzba	Weber number	Arcoumanis et al.	Weber number
1. Vibrational	≈ 12	1. Vibrational	≈ 12
2. Bag	< 20	2. Bag	< 18
3. Bag-streamer	< 50	3. Bag	< 45
4. Stripping	< 100	4. Chaotic breakup	< 100
5. Catastrophic	> 100	5. Sheet stripping	< 350
		6. Wave crest stripping	< 1000
		7. Catastrophic	> 1000

The Reitz-Diwakar breakup model works based on two different assumptions. The first is that atomization and drop breakup near the nozzle within the spray cloud are considered to be indistinguishable, thus the blob method is used to represent the jet breakup into the first spray droplets. In this model, a detailed simulation of the phenomena near the nozzle is replaced by the injection of big spherical droplets, which have a uniform diameter, similar to the nozzle hole size. The injected big droplets are then subject to secondary breakup as they travel through the gaseous medium. Equation 13 shows how $\mathrm{We_P}$ is calculated, where ρ_l and $\mathrm{D_P}$ are the density and diameter of the liquid parcel, $\mathrm{u_{rel}}$ is the relative velocity to the gas phase and σ is the surface tension.

$$We_P = \frac{\rho_l {u_{rel}}^2 D_P}{\sigma} \tag{13}$$

The second assumption is that secondary breakup can be distinguished between two droplet regimes, the bag breakup and the stripping breakup. Bag breakup will occur only if $\mathrm{We_P}$ is greater than a certain value, which is defined to be the bag constant. Reitz (1987) recommends $\mathrm{C_{bag}} = 6$. For higher u_{rel}, stripping-breakup may occur when $We > Cstrip * \sqrt{Re}$, in which C_{strip} is the stripping constant and its recommend value is 0.5. Independent on the breakup regime, the reduction of the particle radius is described by Eq. 14, in which r_P is the particle radius and r_{stable} is the particle new stable radius after breakup.

$$\frac{dr_P}{dt} = \frac{-(r_P - r_{stable})}{\tau_{br}} \tag{14}$$

The characteristic breakup time τ_{br} for bag and stripping breakup are given by (Eq. 15), in which C_1 and C_2 are constant models. Variables ρ_P and ρ_g are liquid and gas density, respectively.

$$\tau_{br-bag} = C_1\sqrt{\frac{\rho_P {r_P}^3}{2\sigma}} \qquad and \qquad \tau_{br-stripping} = C_2\frac{r}{u_{rel}}\sqrt{\frac{\rho_P}{\rho_g}} \tag{15}$$

The new stable particle radius after breakup is given by Eq. 16 for both bag and stripping breakup.

$$r_{stable-bag} = \frac{6\sigma}{\rho_g {u_{rel}}^2}\,C_1 \qquad and \qquad r_{stable-stripping} = \sigma^2/(2{\rho_g}^2{u_{rel}}^3\nu) \tag{16}$$

In Beale & Reitz (1999), an improved spray atomization model is proposed, postulating that droplet breakup is caused by the growing of waves on its surface. The model can be applied in both diesel and gasoline sprays in two distinct steps. In the first, primary breakup is predicted by the Kelvin-Helmholtz (KH) instability model and the diameters of the first droplets ("blobs") are derived. In the following, secondary breakup is predicted with the Kelvin-Helmholtz instability model in conjunction with the Rayleigh-Taylor (RT) accelerative instability model.

The KH frequency and KH wavelength of the fastest-growing wave are shown in Eq. 17, where $Z = \sqrt{We_l}/Re_l$ is the Ohnesorge number, $T = Z\sqrt{We_g}$ is the Taylor number, Re_l is the liquid Reynolds number, We_l is the liquid Weber number and We_g is the gas Weber number.

$$\Omega_{KH}\frac{0.34 + 0.38{We_g}^{1.5}}{(1+Z)(1+1.4T^{0.6})}\sqrt{\frac{\sigma}{\rho_P r^3}} \qquad and \qquad \Lambda_{KH} = \frac{9.02r(1+0.45\sqrt{Z})(1+0.4T^{0.7})}{\left(1+0.865{We_g}^{1.67}\right)^{0.6}} \tag{17}$$

The RT is also a wave instability on the drop surface and the frequency of its fastest-growing wave is given by Eq. 18. Where g_t is the acceleration in the direction of travel. The corresponding wave number K_{RT} is also shown in Eq. 18.

$$\Omega_{RT} = \sqrt{\frac{2}{3\sqrt{3\sigma}}\frac{[-g_t(\rho_P-\rho_g)]^{3/2}}{\rho_P+\rho_g}} \qquad and \qquad K_{RT} = \sqrt{\frac{-g_t(\rho_P-\rho_g)}{3\sigma}} \tag{18}$$

The KH breakup time τ_{KH} is calculated as defined by Eq. 19. In case of secondary breakup, the wavelength related to the fastest-growing wave from RT instabilities is $2\pi C_{RT}/K_{CRT}$ and must be compared to the radius of the droplet. If the wavelength is smaller than the droplet diameter, RT waves are assumed to be growing on the droplet surface. The RT breakup time τ_{RT} can then be calculated as shown in Eq. 19.

$$\tau_{br-KH} = \frac{3.726B_1 r}{\Omega_{KH}\Lambda_{KH}} \qquad and \qquad \tau_{br-RT} = \frac{C_\tau}{\Omega_{RT}} \tag{19}$$

Finally, the new stable particle radius is calculated by r_{c-KH} when the KH model is taking place or by r_{c-RT} when the RT model is in use, both shown in Eq. 20. Equation 14 is also used here to calculate the reduction of the particle radius, independent on the model applied (KH or RT).

$$r_{c-KH} = B_0\Lambda_{KH} \qquad and \qquad r_{c-RT} = \frac{\pi C_{RT}}{K_{RT}} \tag{20}$$

In the previous equations, B_1, C_τ, B_0 and C_{RT} are model constants. In the present work, constants $B_0 = 0.61$ and $B_1 = 20$ were not varied, whereas constants C_τ and C_{RT} were available for change.

3. NUMERICAL SETUP

The open-source tool box OpenFOAM in the version 3.0.x, was chosen for the spray simulations. The computational domain of the spray simulation is a box with dimensions 36 mm in x-direction, 36 mm in y-direction and 60 mm in z (spray cloud axial axis). The grid has equidistant hexahedral cells with a resolution of 0.5 mm, which gives a total of 622.080 cell elements. To avoid stability problems induced by the high velocities present at the injector nozzle, total diminishing variation (TVD) schemes were used for the solution of the convective terms of the governing equations. The implicit second-order backward scheme was used for the time integration and the standard $k-\epsilon$ RANS model was employed for the turbulence. Two breakup models were tested, each one with five different variations (constants were varied). Adjustable time step was set to a maximum CFL = 0.1 and the simulation total time was set to 0.002 s. Finally, the duration of each spray simulation was of approximately one day, using 12 CPUs provided by the Energy Department at the UNESP - Guaratinguetá.

3.1 Test-case: ECN "Spray G"

The test-case chosen to validate this work is the "Spray G" from ECN (Engine Combustion Network), where a multi-hole gasoline spray injection system was used. The operating conditions are summarized in Table 2 and Fig. 3 illustrates the spray cloud formed during the injection. Some experimental and modeling data is available for this test-case, which is used for the validation of the present model. As the purpose of this work is a preliminary study to evaluate the best models and their constants of the given test-case under engine conditions, only one jet from the eight was simulated (see Fig. 3). In the future, after defining the best parameters for this spray, simulation of the full spray (8 jets) will be performed, giving us the chance to analyse other effects like the jet-to-jet interaction.

Table 2: "Spray G" ECN (2015)

Fuel	Iso-octane
Injection pressure	20 MPa
Fuel temperature	90 °C (363 K)
Ambient temperature	300 °C (573 K)
Ambient density	3.5 $\mathrm{kg/m^3}$
Ambient pressure	6 bar (600 kPa)
Ambient composition	89.71% N_2, 6.52% CO_2, 3.77% H_2O
Injected quantity	10 mg
Injection duration	780 μs
Number of nozzle holes	8 (equally spaced)
Hole diameter	165 μm
Fully included angle	80°

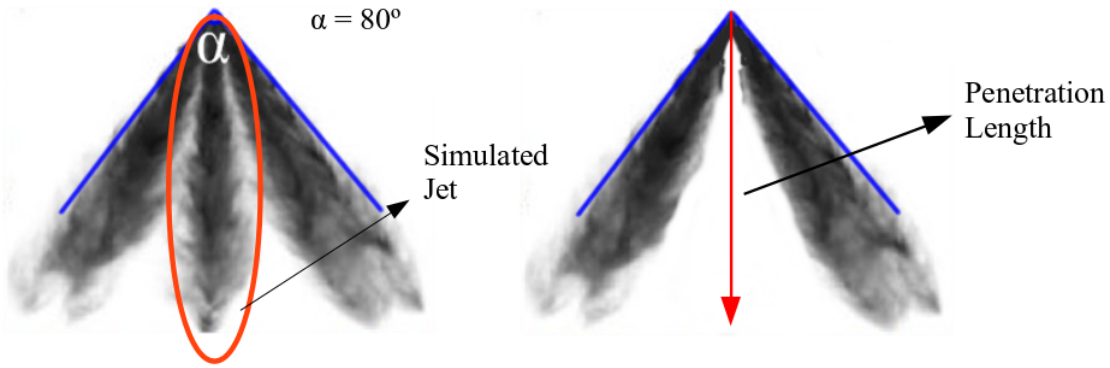

Figure 3: "Spray G" ECN (2015). Circled in red, detail of the simulated single jet

4. RESULTS AND DISCUSSION

In Fig. 3 it was shown how the spray penetration length is defined by the Engine Combustion Network (ECN). Before results can be discussed, the reader should pay attention to the fact that the penetration length is measured on the vertical axis (z) rather than along the spray longitudinal axis. The measured angle between the vertical and spray longitudinal axis is 37 degrees.

Simulations were performed in two different sets. The first using the Reitz-Diwakar and the second using the Reitz-KHRT breakup model. Each set of simulations had five distinct variations with different model constants. Only the best results from each are shown here. The first result to be discussed is the spray penetration length of both liquid and vapour phases, shown in Fig. 4a (using the Reitz-Diwakar model) and Fig. 4b (using the Reitz-KHRT model). As we can see from the penetration curves, simulation results for vapour penetration length agree quite well with measured results during the whole simulation time for both breakup models. On the other hand, liquid length results agree with measured results until the end of injection at 0.78 ms after start of ignition (ASOI). A few milliseconds after injection end, there is a tendency to over predict the measured values in both models. The error is more pronounced using the Reitz-KHRT model. However, the rough reduction trend until total liquid vanishing is well represented using both models.

The more pronounced delayed behaviour of the liquid penetration curve using the KHRT model may be explained by primary breakup producing some bigger droplets, that will travel longer until further breakup regimes and the evaporation process take place. This hypothesis is corroborated by plots of parcels diameter size.

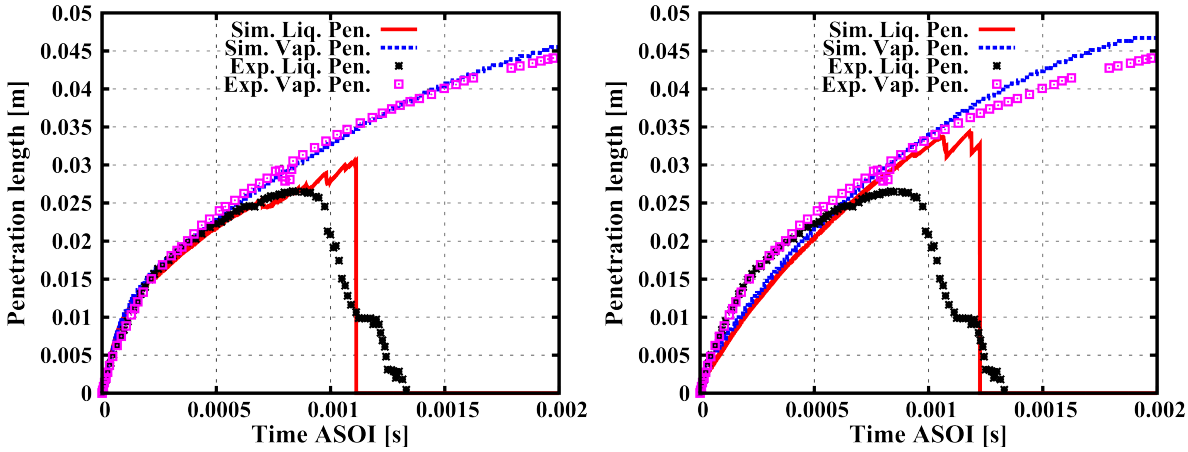

(a) Reitz-Diwakar model (b) Reitz-KHRT model

Figure 4: Spray penetration length - liquid and vapour phase (Simulation vs. Experiments)

Furthermore, in Fig. 5 it is plotted the maximum diameter and Sauter-mean diameter of the parcels within time. In both models, Reitz-Diwakar (Fig. 5a) and Reitz-KHRT (Fig. 5b), the maximum diameter size remains approximately constant around 100 μm and the SMD decreases rapidly just after start of injection until values around 10 μm using Reitz-Diwakar and around 2 μm using Reitz-KHRT. When the latter model is in use, however, a few parcels with much bigger diameter size can be found until end of injection. This is indication of too big parcels being produced by primary breakup (KH instabilities) and may be an explanation for the more pronounced error of this model to predict liquid penetration. Figure 6 presents on the same plot the evaporated mass in kg and the number of parcels within time. The number of parcels reaches a maximum at 0.5 ms and the isoctane liquid mass get fully evaporated before 1 ms using the Reitz-Diwakar model (Fig. 6a), whereas the maximum number of parcels using the Reitz-KHRT model reaches its peak at 0.75 ms and the isoctane is fully evaporated just after 1 ms (Fig. 6b).

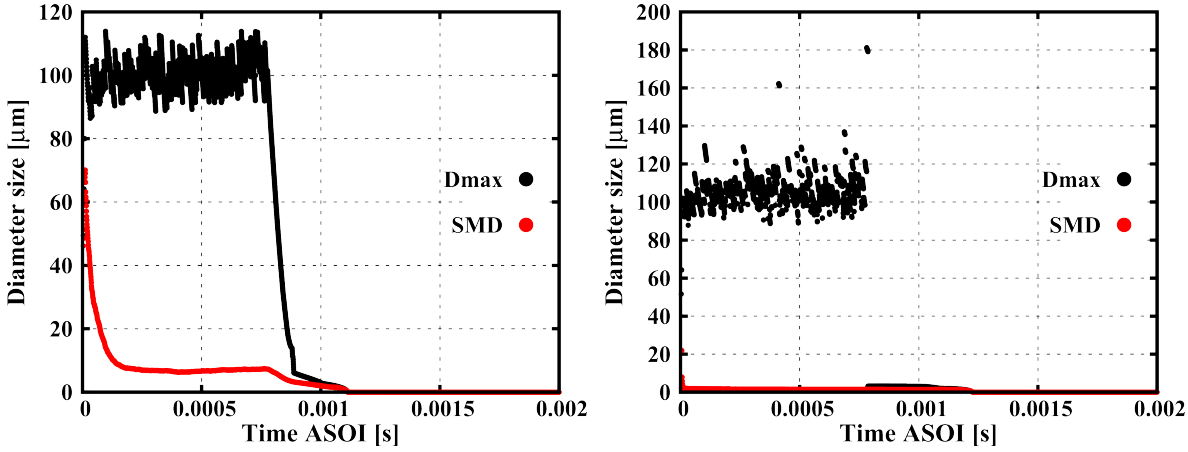

(a) Reitz-Diwakar model (b) Reitz-KHRT model

Figure 5: Maximum diameter and Sauter-Mean Diameter

As at the time there is no iso-octane mixture fraction data available from experiments, mixture fraction results are compared with results from one jet from a full 8-jet spray simulation performed at the Polytechnic University of Milano (Polimi, ECN (2014)) in Fig. 7. The mixture fraction values are taken along the spray longitudinal axis at 0.6 ms after start of injection and the breakup model used in the Polimi simulations was the one proposed by Pilch & Erdman (1987).

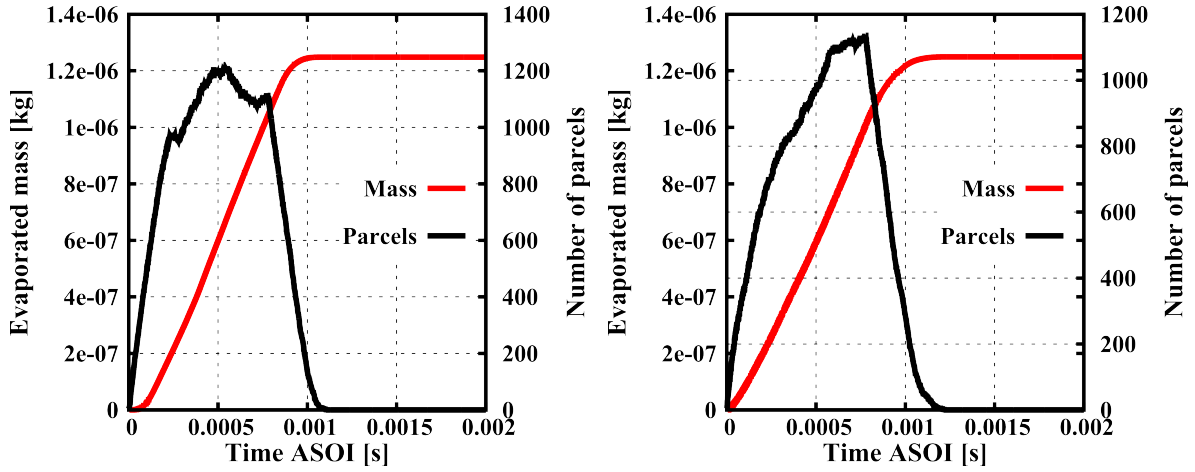

(a) Reitz-Diwakar model (b) Reitz-KHRT model

Figure 6: Evaporated mass and number of parcels

By analysing the iso-octane mixture fraction plots of both simulations, it is possible to see that results agree better with those obtained by Polimi when the Reitz-model is in use (Fig. 7a) rather than when the Reitz-KHRT is employed (Fig. 7b). The first behaviour seems to be more physically real than the latter, i.e., low concentrations of vapour iso-octane are expected near injector nozzle since the fuel did not have enough time to interact with the gas phase, change heat and evaporate. However, this concentration should increase gradually once we look further along the spray axis until a maximum value is reached at the spray tip.

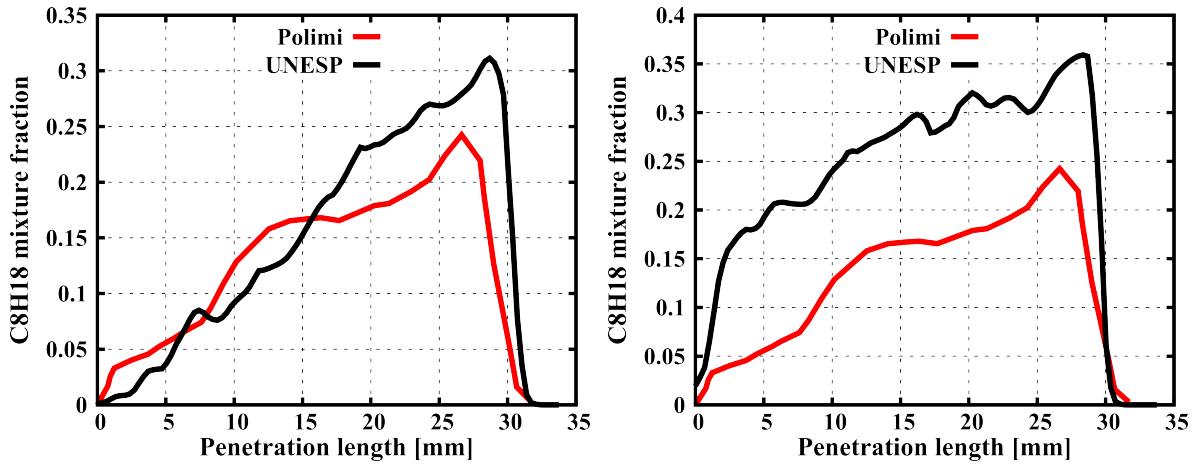

(a) Reitz-Diwakar model (b) Reitz-KHRT model

Figure 7: Iso-octane mixture fraction comparison with Polimi simulations at 0.6 ms ASOI

5. CONCLUSIONS

Fuel-spray simulations of one single jet from the ECN "Spray G" test case were performed using a RANS-LPT framework and OpenFOAM-3.0.x to model the injection of discrete fuel droplets in a gas environment and their related phenomena (momentum exchange, heat and mass transfer and evaporation). Two distinct breakup models (Reitz-Diwakar and Reitz-KHRT) were tested during this preliminary study and results of these simulations were compared and validated with experimental and simulation data provided by ECN. Better agreement with available validation data was achieved using the Reitz-Diwakar model. Further development and model testing must be carried out in order to define best practices for simulating the full 8-jet "Spray G" evaporative test case in a future phase. In that case, the authors aim to investigate other breakup and turbulence models, perform a mesh sensitivity study and study other phenomena not yet investigated as droplet collision and jet to jet interaction.

ACKNOWLEDGEMENTS

The authors acknowledge the financial support by FAPESP (Process 2015/10299-9) and the Energy Department from UNESP-Guaratinguetá for providing the computational resources.

6. REFERENCES

Adachi, M, McDonell, V. G., Tanaka, D, Senda, J, & Fujimoto, H, 1997. Characterization of Fuel Vapor Concentration Inside a Flash Boiling Spray. *SAE Technical Paper*, no. 970871.

Baumgarten, C., 2005. Mixture Formation in Internal Combustion Engines. Springer.

Beale, J. C. & Reitz, R. D., 1999. Modeling Spray Atomization with the Kelvin-Helmholtz/Rayleigh-Taylor Hybrid Model. *Atomization and Sprays*, vol. 9, pp. 623–650.

ECN, 2014. ECN 3rd Workshop Proceedings. URL: `http://www.sandia.gov/ecn/workshop/ECN3.php`.

ECN, 2015. Spray G operation conditions. URL: `http://www.sandia.gov/ecn/G/targetCondition/sprayG.php`.

Goryntsev, D, Sadiki, A, Klein, M, & Janicka, J, 2010. Analysis of cyclic variations of liquid fuel-air mixing processes in a realistic DISI IC-engine using Large Eddy Simulation. *International Journal of Heat and Fluid Flow*, vol. 31, pp. 845–849.

Jangi, M, Solsjo, R, Johansson, B, & Bai, X, 2015. On large eddy simulation of diesel spray for internal combustion engines. *International Journal of Heat and Fluid Flow*, vol. 53, pp. 68–80.

Lucchini, T, D'Errico, G, & Ettorre, D, 2011. Numerical investigation of the spray-mesh-turbulence interactions for high-pressure, evaporating sprays at engine conditions. *International Journal of Heat and Fluid Flow*, vol. 32, pp. 285–297.

Marshall, W. R. & Ranz, W. E., 1952. Internal Combustion Engine Modeling. Hemisphere Publishing.

Peterson, B., Reuss, D. L., & Sick, V., 2014. On the ignition and flame development in a spray-guided direct-injection spark-ignition engine. *Combustion and Flame*, vol. 161, pp. 240–255.

Pilch, M & Erdman, C. A., 1987. Use of Breakup Time Data and Velocity History Data to Predict The Maximum Size Of Stable Fragments For Acceleration-Induced Breakup Of A Liquid Drop. *Int. J. Multiphase Flow*, vol. 13, pp. 741–757.

Pope, S. B., 2011. Simple models of turbulent flows. *Physics of Fluids*, vol. 23.

Reitz, R. D. & Bracco, F. V., 1986. The Encyclopedia of Fluid Mechanics. Gulf Publishing.

Reitz, R. D., 1987. Modeling Atomization Processes in High-Pressure Vaporizing Sprays. *Atomisation and Spray Technology*, vol. 3, pp. 309–337.

Subramaniam, S., 2013. Lagrangian-Eulerian methods for multiphase flows. *Progress in Energy and Combustion Science*, vol. 39, pp. 215–245.

The International Council on Clean Transportation, 2014. EU CO2 Emission Standards for Passenger Cars and Light-comercial vehicles. In: Berlin.

Vuorinen, V. A., Hillamo, H, Kaario, O, Nuutinen, M, Larmi, M, & Fuchs, L, 2011. Effect of Droplet Size and Atomization on Spray Formation: A Priori Study Using Large-Eddy Simulation. *Flow Turbulence Combust*, vol. 86, pp. 533–561.

Westbrook, C. K., Mizobuchi, Y., Poinsot, T. J., Smith, P. J., & Warnatz, J., 2005. Computational combustion. *Proceedings of the Combustion Institute*, vol. 30, pp. 125–157.

Wierzba, A, 1990. Deformation and breakup of liquid drops in a gas stream at nearly critical Weber numbers. *Experiments in Fluids*, vol. 9, pp. 59–64.

Yang, J. L. & Anderson, R. W., 1998. Fuel Injection Strategies to Increase Full-Load Torque Output of a Direct-injection SI Engine. *SAE Technical Paper*, no. 980495.

Zheng, Z., Tian, X., & Zhang, X., 2015. Effects of split injection proportion and the second injection time on the mixture formation in a GDI engine under catalyst heating mode using stratified charge strategy. *Applied Thermal Engineering*, vol. 84, pp. 237–245.

Zuo, B, Gomes, A. M., & Rutland, C. J., 2000. Modelling superheated fuel sprays and vaporization. *Int J Engine Research*, vol. 1, pp. 321–336.